Korean J. Chem. Eng., 34(6), 1874-1881 (2017)
DOI: 10.1007/s11814-017-0085-2

pISSN: 0256-1115
eISSN: 1975-7220

Poisoning effect of CaO on CeO_2/TiO_2 catalysts for selective catalytic reduction of NO with NH_3

Ye Jiang†, Xuechong Wang, Changzhong Bao, Shanbo Huang, Xiuxia Zhang, and Xinwei Wang

College of Pipeline and Civil Engineering, China University of Petroleum,
No. 66 Changjiang West Road, Qingdao 266580, China
(*Received 15 July 2016 • accepted 20 March 2017*)

Abstract−The effect of CaO on CeO_2/TiO_2 catalysts prepared by a single step sol-gel method for selective catalytic reduction of NO with NH_3 was investigated. The results showed that CaO could severely deactivate the CeO_2/TiO_2 catalysts. Based on the characterization results obtained by BET, XRD, XPS, H_2-TPR and NH_3-TPD, the deactivation by CaO of CeO_2/TiO_2 catalysts should be attributed to pore blockage, lower concentration of Ce on catalyst surface, reduction of Ce^{3+} and surface adsorbed oxygen, degradation of redox ability and decrease in NH_3 adsorption capacity. The theoretical DFT results demonstrated that Ca atom could strongly interact with cerium oxygen, which inhibits the formation and hydrogenation of oxygen vacancies on catalyst surface.

Keywords: Selective Catalytic Reduction, CaO, CeO_2/TiO_2, Single Step Sol-gel Method, DFT

INTRODUCTION

Selective catalytic reduction (SCR) of NO_x with NH_3 is a well-proven technique for NO_x removal in stationary sources. Even though vanadia-based catalysts have been widely used industrially during the past decades, there are several drawbacks associated with this type of catalyst, such as toxicity of vanadium species, high oxidization activity of SO_2 to SO_3 [1], formation of N_2O at high temperatures [2] and catalyst deactivation by the exposure to ash compounds present in the flue gas. In recent years, cerium-based catalysts have been regarded as a promising candidate for vanadia-based catalysts in the NH_3-SCR reaction due to their outstanding oxygen storage capacity and excellent redox property [3-6]. Among these cerium-based catalysts, CeO_2/TiO_2 prepared by different methods were reported to be active for the SCR of NO with NH_3 in the presence of oxygen [7-9].

It is known that vanadia-based catalysts can be deactivated by the deposition of alkaline earth metal compounds in fly ash [10-12]. The effect of alkaline earth metals on the deNO_x performance of vanadia-based catalysts has been studied because of its practical interest. Chen et al. [10] proposed that the poisoning effect of CaO on V_2O_5/TiO_2 catalysts was attributed to its basicity, which could neutralize the acidity of the catalyst surface. Nicosia et al. [11] suggested that Ca occupies the non-atomic hole sites of the (010) V_2O_5 surface over V_2O_5/WO_3-TiO_2 catalysts, such that both Brønsted acid and V^{5+}=O sites are blocked. Tang et al. [12] found that the deactivation by Ca^{2+} ions of V_2O_5/TiO_2 catalysts resulted from the degradation of surface acidity and reducibility. Chen et al. [13] drew a similar conclusion in the study on the poisoning effect of CaO and MgO on V_2O_5-WO_3/TiO_2 SCR catalysts. However, the effect of alkaline earth metals on cerium-based catalysts has been reported by only a few researchers [14,15]. Mousavi et al. [14] found that the loading of Ca caused an obvious decrease in NO conversion over CeO_2-MO_x (M=Mn, Fe). Wang et al. [15] studied the effect of Ca^{2+} ions on Ce/TiO_2 catalysts prepared by wet impregnation method. The growth of ceria nanoparticles, the change in surface acidity and the reduced Ce^{4+}/Ce^{3+} redox cycle rate were proposed to contribute to their deactivation. To our best knowledge, few efforts have been made to investigate the effect of Ca on CeO_2/TiO_2 catalysts prepared by a single step sol-gel method, which were reported to possess excellent SCR activity in the medium temperature range [16].

Our objective was to study the effect of CaO doping on the SCR of NO with NH_3 over CeO_2/TiO_2 catalysts prepared by a single step sol-gel method. These catalysts were characterized by means of BET and pore size distribution measurements, XRD, XPS, H_2-TPR, NH_3-TPD and NO reduction measurements. Density functional theory (DFT) calculations were used to theoretically study the doping of CaO on CeO_2/TiO_2 catalysts at the atomic level. Special attention was paid to explore the substantial changes in CeO_2/TiO_2 catalysts caused by CaO and clarify their CaO-poisoning mechanism.

EXPERIMENTAL

1. Catalyst Preparation

The CeO_2/TiO_2 catalysts with CeO_2 loading of 20 wt% (denoted by CeTi) were prepared by a single step sol-gel method. Butyl titanate (0.1 mol), anhydrous ethanol (3.5 mol), deionized water (1.9 mol), nitric acid (0.2 mol), cerium nitrate (0.01 mol) were mixed under vigorous stirring at room temperature. The mixture was stirred for 3 h, dried at 80 °C for 24 h and then calcined at 500 °C for 6 h.

The CaO-doped catalysts were prepared by impregnating the CeTi catalysts with the aqueous solutions of required concentra-

†To whom correspondence should be addressed.
E-mail: jiangye@upc.edu.cn
‡The paper will be reported in the 11th China-Korea Clean Energy Workshop.

tion of $Ca(NO_3)_2$. The samples were impregnated at room temperature for 4 h, dried at 110 °C for 12 h and then calcined at 500 °C for 6 h. The CaO-doped catalysts were denoted by Ca_xCeTi where x represents the molar ratio of Ca/Ce.

2. Catalytic Activity Measurement

The SCR activity measurements were made in a fixed-bed reactor with a quartz tube (i.d.=8 mm) containing 0.34 g catalyst with 100-250 μm. The typical reactant gas mixture consisted of 0.1 vol% NO, 0.1 vol% NH_3, 3 vol% O_2 and balance gas N_2. The total flow rate was 500 mL/min and the gas hourly space velocity (GHSV) was 90,000 h^{-1}. The concentrations of NO, NO_2 and O_2 were monitored by the flue gas analyzer (350 Pro, Testo). The activity data were collected and recorded after 30 min when the SCR reaction reached a steady state at each temperature.

3. Catalyst Characterization

BET surface area, pore volume and pore size distribution were measured by N_2 adsorption and desorption at liquid nitrogen temperature (−196 °C) with ASAP 2020-M (Micromeritics Instrument Corp.). The X-ray diffraction (XRD) measurement involved an X'Pert PRO MPD system (Panalytical Corp.) with Cu Kα radiation.

The X-ray photoelectron spectrum (XPS) measurements were used to determine the atomic concentration and the state of the elements on catalyst surface by a Thermo ESCALAB 250 spectrometer using monochromated Al Kα X-rays (hv=1,486.6 eV) as a radiation source at 150 W. Sample charging effects were eliminated by correcting the observed spectra with the C 1s binding energy (BE) value of 284.6 eV.

Temperature programmed desorption (NH_3-TPD) and Temperature programmed reduction (H_2-TPR) were performed on a FINESORB-3010 chemisorption analyzer (FINETEC Instruments Corp.) with a thermal conductivity detector (TCD).

4. Computational Details

All calculations were based on DFT by means of Materials Studio (MS) Modeling DMol3 from Accelrys [17]. The (001) surface of anatase TiO_2 has been considered to be important for SCR reaction and widely studied by experimental and theoretical methods [18-20]. In this work, the (001) anatase surface was considered as the catalyst surface. Two layers were used to calculate and all atoms were relaxed. According to the XRD results, CeO_2 crystals were not detected on the CeO_2/TiO_2 catalysts. As a result, the Ce atom replaced Ti atom on the surface layer. The double-numerical plus polarization (DNP) functions and GGA-PBE [21,22] were used for the whole calculations. The core electrons were treated with DFT Semi-core Pseudopots (DSPP) [23]. The real space cutoff radius was sustained as 5.2 Å. A Monkhorst-Pack grid of size of (2×2×1) was applied to the surface Brillouin zone of the whole system. A 20 Å vacuum layer in the z-direction was used to avoid interactions of the surfaces.

All the structures were optimized and the convergence criteria for energy and displacement of geometry optimization were set as 1×10^{-5} Ha and 5×10^{-3} Å, respectively. The Adsorption energies (E_{ad}) of molecule were calculated as follows:

$$E_{adsorption}=E_{system}-E_{cluster}-E_{adsorbate} \quad (1)$$

where E_{system} was the total energy of the cluster with the molecule adsorbed, $E_{cluster}$ was the energy of the cluster, and $E_{adsorbate}$ was the energy of an isolated molecule. Note that more negative adsorption energy indicates a stronger binding of molecule adsorbed on the surface.

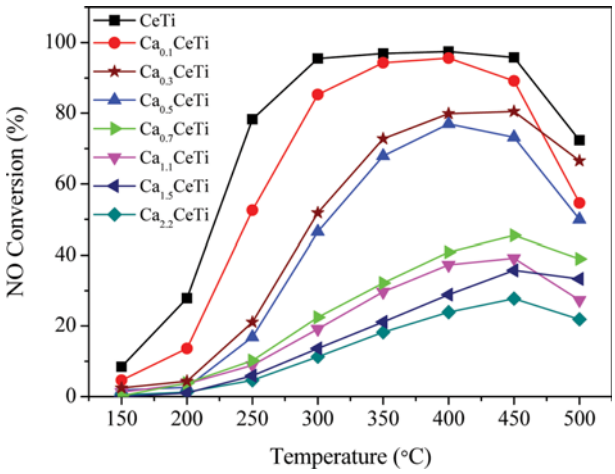

Fig. 1. Variation of NO conversion with temperature over the CeO_2/TiO_2 catalysts with different CaO loadings. Reaction conditions: [NO]=[NH_3]=0.1 vol%, [O_2]=3 vol%, balance N_2 and GHSV=90,000 h^{-1}.

RESULTS AND DISCUSSION

1. The Effect of CaO on Ce-Ti Oxide Catalysts' Activity

Fig. 1 shows the NO conversion as a function of reaction temperature over CeO_2/TiO_2 catalysts with different CaO loadings. The fresh catalyst had the best catalytic activity in the temperature range of 150-500 °C, and nearly 100% NO conversion was obtained at 300-450 °C. When the molar ratio of Ca/Ce was 0.1, the SCR activity deceased slightly. Further increasing CaO loadings caused the tremendous decrease in NO conversion while narrowed the temperature window for SCR reaction noticeably. When the molar ratio of Ca/Ce reached 2.2, the maximum NO conversion was only 27.8%. These results demonstrated that the presence of CaO had a suppressive effect on the SCR activity of CeO_2/TiO_2 catalysts, but the decrease in the activity of the catalysts did not show a linear

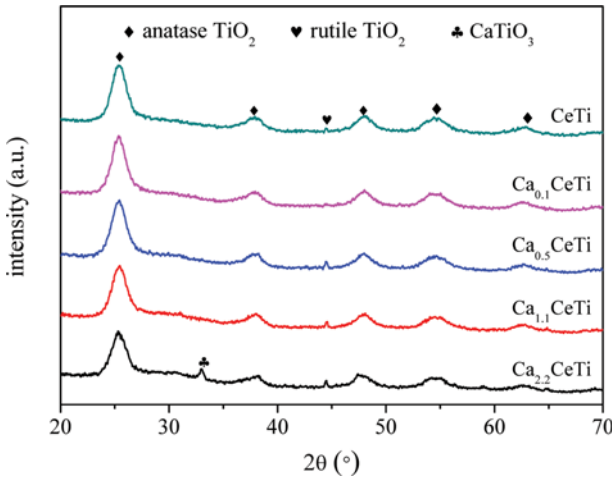

Fig. 2. XRD patterns of different catalyst samples.

dependence on the CaO loadings. Chen et al. [13] also found a similar phenomenon in the study on the poisoning effect of alkali (earth) metals on V_2O_5-WO_3/TiO_2 SCR catalysts.

2. Characterization of Catalysts

2-1. XRD Results

The XRD patterns of CeO_2/TiO_2 catalysts with different CaO loadings are presented in Fig. 2. When the molar ratio of Ca/Ce was lower than 0.5, the characteristic lines of anatase TiO_2 (PDF21-1272) and an extremely weak diffraction peak at about 44.0° ascribed to rutile TiO_2 (PDF21-1276) could be observed. In the TiO_2 phases, anatase was the dominating one. However, the characteristic diffraction peaks due to Ce and Ca species were not detected. This indicated that the presence of CaO did not markedly modify the crystallinity and dispersion of ceria on TiO_2 carrier. Ce and Ca species were well dispersed and existed as amorphous or highly dispersed phases at the surface of TiO_2 and catalyst samples, respectively. As the molar ratio of Ca/Ce exceeded 0.5, the weak diffraction peak due to rutile TiO_2 (PDF21-1276) became a bit bigger while anatase was still the dominant phase. This meant that a little anatase TiO_2 was transformed to the more thermodynamically stable rutile phase. In addition, when the molar ratio of Ca/Ce reached 2.2, a new diffraction peak ascribed to perovskite ($CaTiO_3$) (PDF22-0153) appeared, but cubic CeO_2 remained undetected. By contrast, it was reported that after CaO (Ca/Ce molar ratio=2.0) was doped on Ce/TiO_2 catalysts prepared by wet impregnation method, the transformation of amorphous ceria to cubic CeO_2 was observed [14]. It was clear that the difference in catalyst preparation methods caused the difference in the crystallinity of ceria. Furthermore, it can be also seen from Fig. 2 that the presence of Ca led to a slight decrease in the intensity of the peaks due to anatase TiO_2. Liu et al. [24] also found a similar phenomenon when they studied the effect of Ca doping on MnO_x/TiO_2 catalysts. It was likely because Ca intercalated into TiO_2 lattice, resulting in the expansion of TiO_2 lattice. This also implied that there was a strong interaction between Ca and Ti.

2-2. BET Results

The physical properties of various samples are summarized in Table 1. When the molar ratio of Ca/Ce was 0.1, the BET surface area and total pore volume increased, compared with those of the fresh catalyst. It was likely because there was a certain synergistic effect among Ca, Ce and Ti, leading to the good dispersion of ceria or TiO_2 (as confirmed by XRD results). However, when the molar ratio of Ca/Ce exceeded 0.1, the BET surface area and total pore volume decreased with increasing Ca loadings. The possible reason could be that Ca species deposited on the catalyst surface might block the microspore [24]. The higher Ca loading, the stronger this effect was. The variation caused by different CaO loadings in the physical structure of CeO_2/TiO_2 catalysts was likely to arise from these two opposite effects. However, the catalytic activity of CeO_2/TiO_2 catalysts decreased with increasing Ca loadings (Fig. 1). This suggested that the physical properties of the CeO_2/TiO_2 catalysts seem not to be the most important factor for determining their deactivation by CaO.

Fig. 3 shows the N_2 adsorption-desorption isotherms and pore size distributions of CeO_2/TiO_2 catalysts with different CaO loadings. The N_2 sorption results revealed that all the samples exhibited type IV isotherms (IUPAC classification), indicating the presence of mesopores. The fresh catalyst yielded the pore diameter distribution centered at about 5.9 nm, which was mainly assigned to pore structure of the titania support. With the increase of CaO load-

Table 1. Physical properties of different catalyst samples

Samples	Ca content (wt%)	BET surface area (m^2/g)	Total pore volume (cm^3/g)	Average pore diameter (nm)
CeTi	-	98.55	0.1542	5.1747
$Ca_{0.1}$CeTi	0.540	100.67	0.1775	5.9161
$Ca_{0.5}$CeTi	2.642	86.72	0.1654	6.4635
$Ca_{1.1}$CeTi	5.635	71.81	0.1477	7.0426
$Ca_{2.2}$CeTi	10.688	54.55	0.1281	7.9814

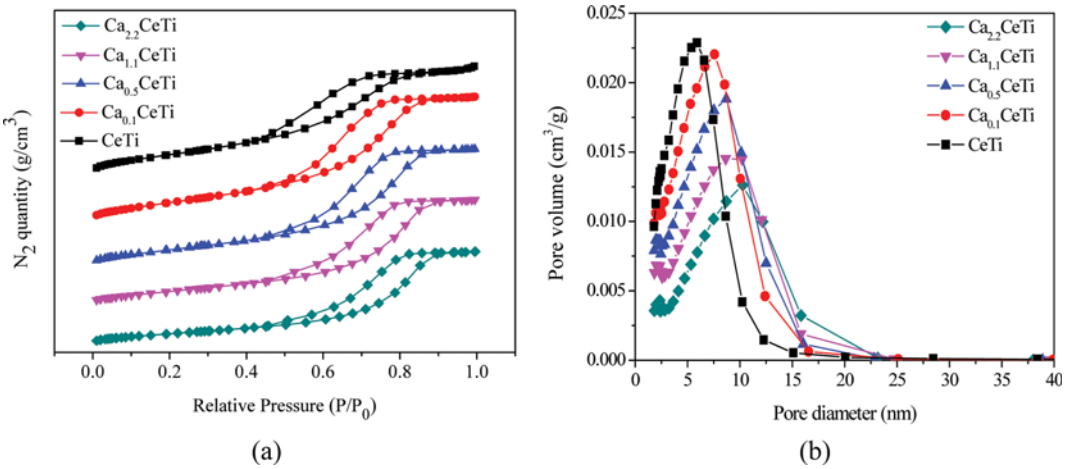

Fig. 3. N_2 sorption isotherms (a) and pore size distribution (b) of different catalyst samples.

ings, the pore sizes of CeO_2/TiO_2 catalysts increased while the pore volumes decreased. This confirmed that a fraction of small mesopores might be blocked. According to XRD results, $CaTiO_3$ was found to form and resulted in the expansion of TiO_2 lattice, which might cause the pore blockage of CeO_2/TiO_2 catalysts, thereby lowering the activity of the catalysts.

2-3. XPS Results

Different catalyst samples were further analyzed using XPS technique to get a better understanding about the chemical state of all elements on the catalyst surface. Table 2 lists the surface atomic concentration of different samples. After the doping of Ca, the concentration of Ce on the catalyst surface decreased with increasing CaO loadings. It was noted that Ce concentration on the surface of different samples was in the same sequence of their catalytic activity. It might be because the lower surface concentration of Ce resulted in lower SCR reaction capacity, contributing to the worse catalytic activity.

Fig. 4 presents Ti 2p, Ce 3d and O 1s XPS spectra of different samples. As shown in Fig. 4(a), the BE values of Ti $2p_{1/2}$ and Ti $2p_{3/2}$ for the fresh catalyst were about 464.4 and 458.6 eV, respectively. This meant that Ti existed as Ti^{4+} but not Ti^{3+}, which was consistent with published values [25,26]. After doping CaO, Ti 2p BE values were changed slightly. It has been demonstrated that the Ti 2p BE values of Ti^{3+} are 1.8 eV lower than those of Ti^{4+} [23]. Therefore, Ti still existed as Ti^{4+} after the doping of CaO. According to the XRD results, $CaTiO_3$ was found to exist in $Ca_{2.2}CeTi$. The handbook of XPS [27] reports that Ti $2p_{3/2}$ binding energy of $CaTiO_3$ is about 458.5 eV. From the XPS results, we speculated that $CaTiO_3$ might form on $Ca_{1.1}CeTi$ and $Ca_{2.2}CeTi$. However, the XRD results show that $CaTiO_3$ was not detected in $Ca_{1.1}CeTi$. It seemed that $CaTiO_3$

Table 2. Surface atomic concentrations of different samples

Samples	Ca (%)	Ti (%)	Ce (%)	Ce^{3+} (%)	O_T (%)	O/O_T (%)		
				$Ce^{3+}+Ce^{4+}$		O_α/O_T	O_β/O_T	O_γ/O_T
CeTi	-	23.3	3.4	28.4	73.3	69.6	23.8	6.6
$Ca_{0.1}CeTi$	0.9	24.5	2.8	23.5	71.8	76.3	21.1	2.6
$Ca_{0.5}CeTi$	3.0	22.5	2.5	22.0	72.0	72.3	20.1	7.6
$Ca_{1.1}CeTi$	4.3	20.8	2.0	20.4	72.9	68.2	17.2	14.6
$Ca_{2.2}CeTi$	6.5	19.5	1.9	18.1	72.1	69.3	16.0	14.7

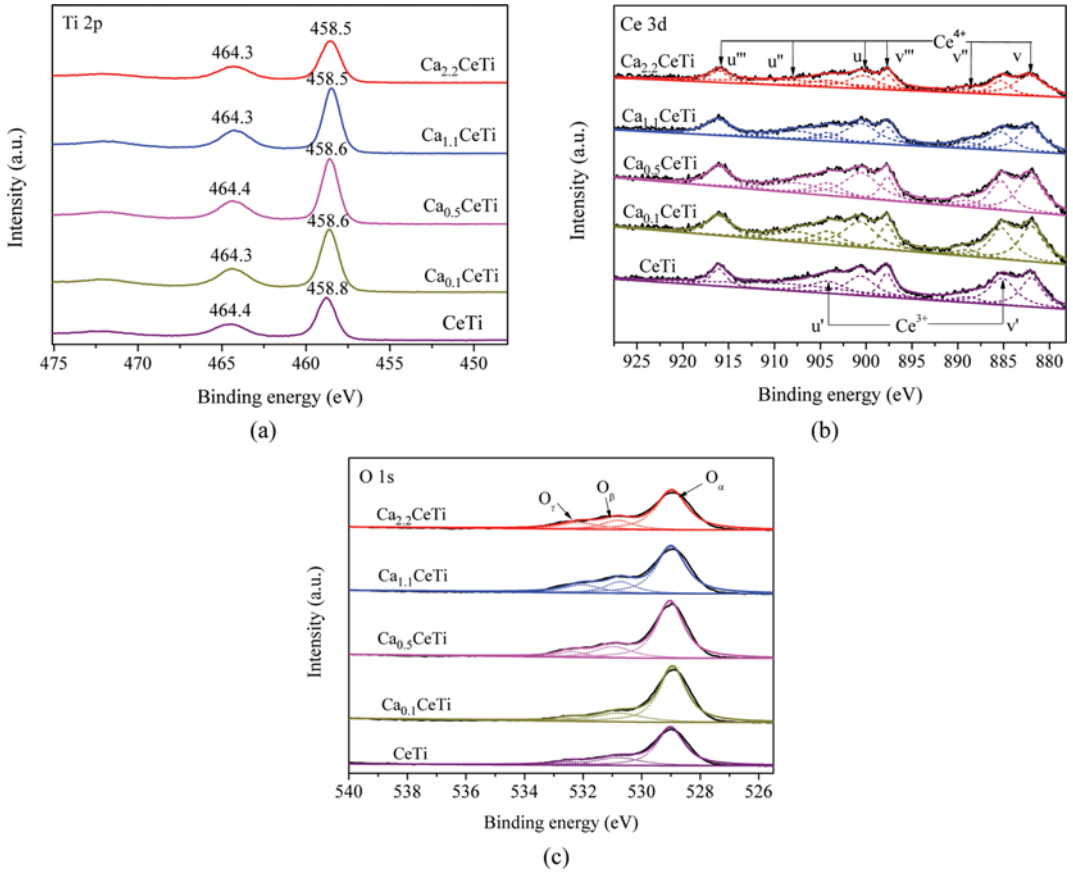

Fig. 4. XPS spectra of the Ti 2p (a), Ce 3d (b), and O 1s (c) region.

was highly dispersed or amorphous in structure. This also indicated that there existed a strong interaction between Ca and Ti.

The complicated Ce 3d XPS spectra are presented in Fig. 4(b). The u′ and v′ peaks were attributed to Ce^{3+} species, while the u‴, u″, u and v‴, v″, v peaks belonged to Ce^{4+} species [16,28-30]. According to the area ratio of peaks representing Ce^{3+} and Ce^{4+} species, the ratio of $Ce^{3+}/(Ce^{3+}+Ce^{4+})$ could be calculated and is summarized in Table 2. The ratio of $Ce^{3+}/(Ce^{3+}+Ce^{4+})$ decreased with increasing CaO loadings. It was clear that the doping of CaO led to the decrease in the amount of Ce^{3+} and the increase in the amount of Ce^{4+}, i.e., a proportion of Ce^{3+} was transformed into Ce^{4+} due to the presence of CaO. This might be attributed to the fact that the interaction between Ca and Ce promoted the transformation of Ce^{3+} into Ce^{4+}. However, Wang et al. [15] found that Ce^{3+} disappeared completely after CaO (the molar ratio of Ca/Ce=1) was doped on Ce/TiO_2 catalyst prepared by wet impregnation method. It is widely accepted that Ce^{3+} plays a crucial role in the excellent activity of Ce/TiO_2 catalysts. This meant that CeO_2/TiO_2 catalysts prepared by a single step sol-gel method seem to have better resistance against CaO. Ce^{3+} is believed to be capable of creating a charge imbalance, vacancies and unsaturated chemical bonds on the catalyst surface, which leads to the increase in chemisorbed oxygen or/and weakly bonded oxygen species on the catalyst surface [31]. In addition, Ce^{3+} has a positive effect on the redox ability and adsorption of NO or NH_3 [32]. Accordingly, the decrease in the amount of Ce^{3+} might be one of the main reasons for the deactivation by CaO of the CeO_2/TiO_2 catalysts.

The O 1s XPS spectra of different samples can be fitted into three overlapping peaks, as shown in Fig. 4(c). The sub-bands at 529.0-530.0 eV could be attributed to the lattice oxygen in the metal oxides (denoted as O_α) [16,28-30], and two shoulder sub-bands are assigned to the surface adsorbed oxygen (denoted as O_β) and surface oxygen by hydroxyl species or adsorbed water species as contaminants at the surface (denoted as O_γ), respectively [16,28-31]. O_β ratio, which was calculated by $O_\beta/(O_\alpha+O_\beta+O_\gamma)$, is listed in Table 2. O_β ratio decreased from 23.8% to 16.0% when the molar ratio of Ca/Ce increased from 0 to 2.2. Surface adsorbed oxygen (O_β) is reported to be more reactive in oxidation reactions due to its higher mobility than lattice oxygen (O_α) [28]. High O_β ratio is considered to be beneficial for the NO oxidation to NO_2 in the SCR reaction [33,34]. Consequently, it could be inferred that the decrease in surface adsorbed oxygen had a negative impact on the SCR reaction. It is worth mentioning that the results of the activity tests were consistent with this conclusion.

2-4. H_2-TPR Results

H_2-TPR experiments were performed to evaluate the effect of CaO on the redox ability of CeO_2/TiO_2 catalysts. In this work, the reduction peak temperature (T_{red}) was taken as a measure of the reducibility of the catalyst system. The higher T_{red} is, the weaker is the redox ability of the catalyst [35]. The H_2-TPR profiles of different catalysts are illustrated in Fig. 5. The fresh catalyst presented a broad peak centered at 522 °C and the onset temperature (T_{onset}) was about 271 °C, which is similar to that reported by Li et al. [36]. This peak could be attributed to the reduction of surface oxygen species of ceria [37,38]. The reduction of bulk ceria did not take place in the temperature range of 300-600 °C, since it occurred only

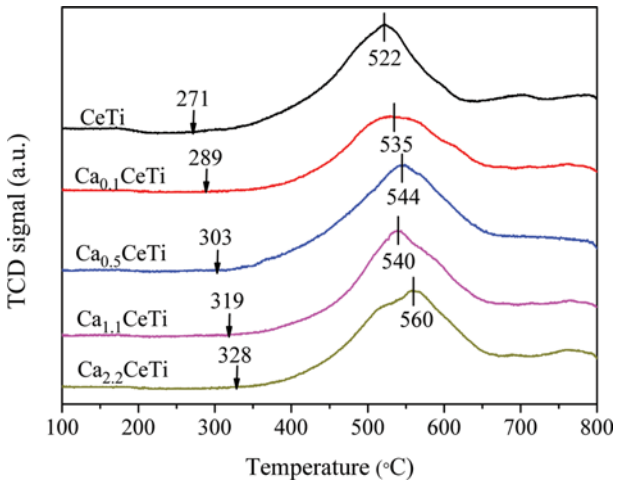

Fig. 5. H_2-TPR profiles of different catalyst samples.

above 750 °C [39]. As for the CaO-doped CeO_2/TiO_2 catalysts, T_{onset} shifted to higher temperature with increasing the CaO loadings while T_{red} displayed the same tendency. This implied that Ca interacted with Ce species and then inhibited the redox reaction. It was noted that the decrease in the redox abilities of CeO_2/TiO_2 catalysts after the doping of CaO was in accordance with the results of XPS and the activity tests.

2-5. NH_3-TPD Results

Fig. 6 shows the NH_3-TPD profiles of different catalyst samples. The amount of NH_3 desorbed on the CaO-doped CeO_2/TiO_2 catalysts showed a decreasing tendency with increasing the CaO loadings. This implied that the surface acidity of the catalyst was neutralized by CaO, thereby causing a decline in the NH_3 adsorption capacity. It has been established that NH_3 adsorption is crucial for the SCR reaction [40]. The sequence in the amount of the desorbed NH_3 was in good agreement with the SCR activity of these catalysts. However, when the molar ratio of Ca/Ce exceeded 0.5, the surface acidity decreased less seriously than the SCR activity. This indicated that the surface acidity made a strong impact on the SCR activity for the CaO-doped CeO_2/TiO_2 catalysts, but they

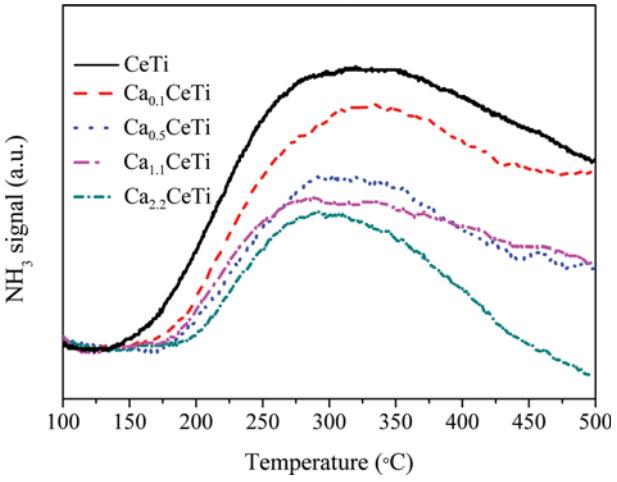

Fig. 6. NH_3-TPD profiles of different catalyst samples.

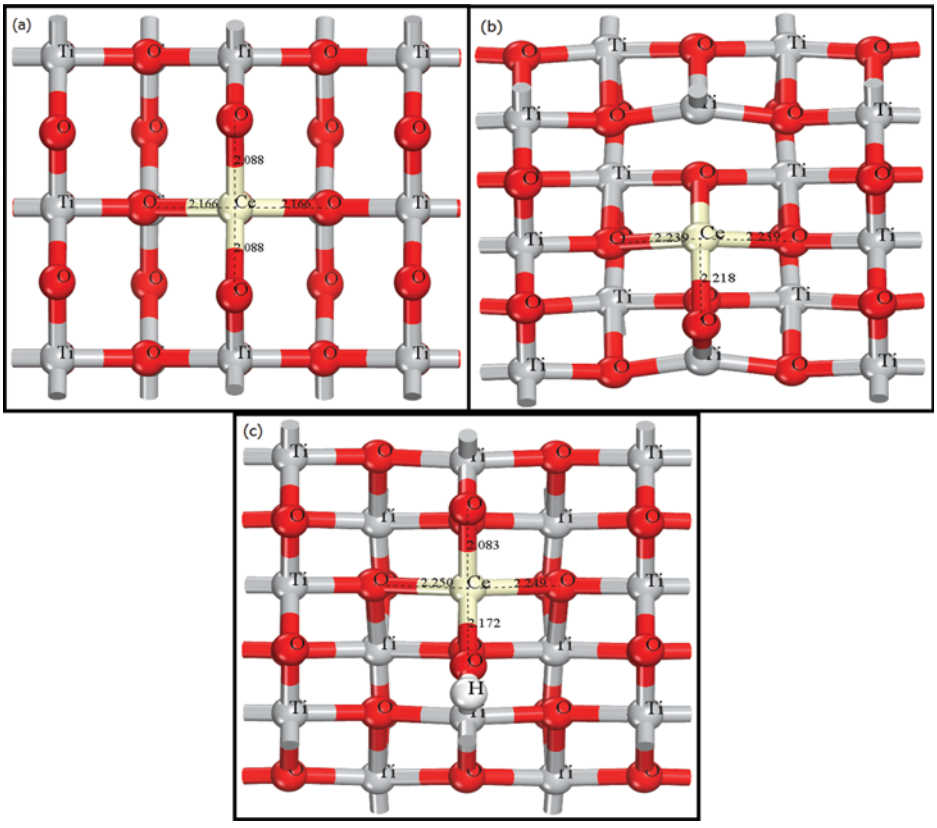

Fig. 7. Optimized structures of CeO_2/TiO_2 (a), oxygen-captured CeO_2/TiO_2 (b), hydrogenated CeO_2/TiO_2 (c).

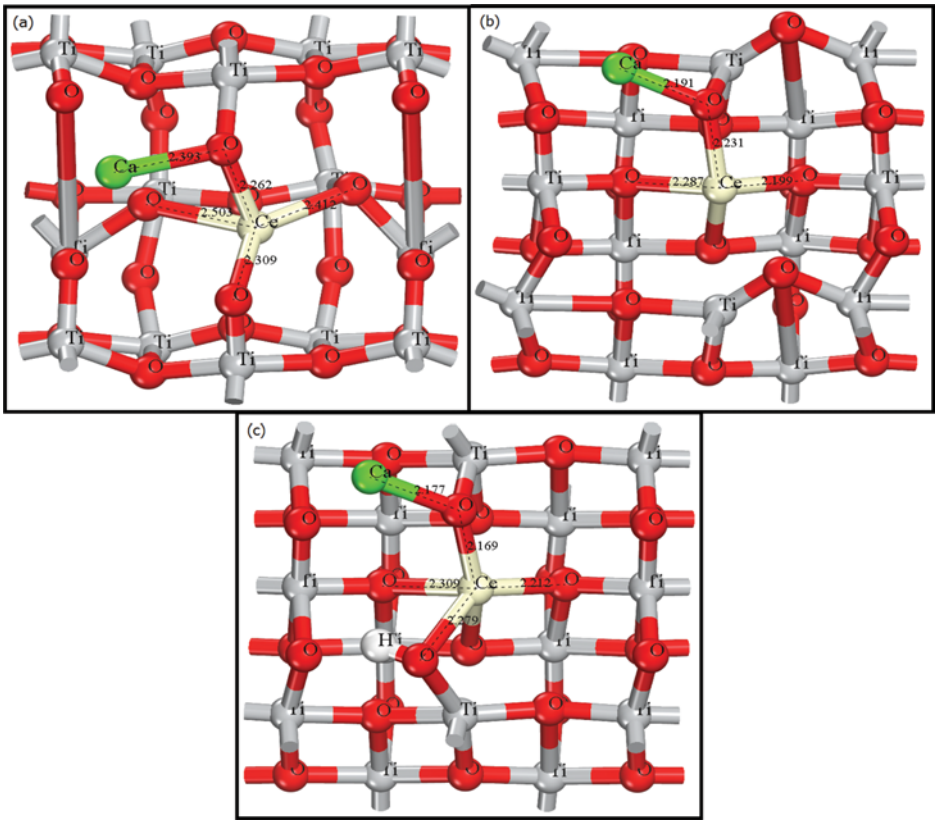

Fig. 8. Optimized structures of Ca doped CeO_2/TiO_2 (a), oxygen-captured Ca doped CeO_2/TiO_2 (b), hydrogenated Ca doped CeO_2/TiO_2 (c).

were not linearly related.

2-6. DFT Calculations

NH_3-TPD results showed that the doping of CaO led to the decrease in the adsorbed NH_3 on CeO_2/TiO_2 catalysts. Accordingly, we used the DFT calculations to study the interaction between Ca and the CeO_2/TiO_2 catalyst at the atomic level. The optimized structures of the fresh and Ca-doped CeO_2/TiO_2 models are shown in Figs. 7-8. According to the calculated structures, it is obvious that the surfaces of CeO_2/TiO_2 (001) are significantly changed after the doping of Ca. Ca atom is bonded to the oxygen atom adjacent to the cerium atom (the bond length of Ca-O is 2.393 Å), which means that Ca is strongly adsorbed on the surfaces. The length of Ce-O bond extends from 2.088 Å to 2.309 Å and 2.262 Å, respectively. It is because the electron transfers from the Ca atom, which satisfies the electron orbit of the cerium oxide and consequently weakens the interaction between O and Ce. As for the fresh CeO_2/TiO_2 catalyst, the formation of an oxygen vacancy requires 137.81 kcal/mol, and the energy of exothermic hydrogenation is −114.97 kcal/mol. However, the creation of an oxygen vacancy in the Ca-doped CeO_2/TiO_2 catalyst costs 157.86 kcal/mol, which is much higher than that in the fresh CeO_2/TiO_2 catalyst. It is known that the lower energy of oxygen vacancy creation will cause a decrease in the proportion of Ce^{3+} [41], which is in accordance with the XPS results. In addition, the interaction of Ca and cerium oxygen was found to inhibit hydrogenation and the energy of hydrogenation is −92.94 kcal/mol in the Ca-doped CeO_2/TiO_2 model, compared with that of fresh CeO_2/TiO_2 catalyst. The Mulliken charge of cerium for the fresh CeO_2/TiO_2 (001) surface is +2.027. However, in the Ca-doped model, the charge of the cerium changed to +1.894 and Ca had a charge of +1.572, which makes more cerium ionized. The ionization of the cerium ionized the oxygen atoms of the around cerium. The ionization of the oxygen makes the formation of the oxygen vacancy harder. The oxygen vacancy is important for SCR reaction. The Ca doping has a negative effect on the creation of oxygen vacancies, which is proved by the lower energy of oxygen vacancy creation.

CONCLUSIONS

The doping of CaO resulted in serious deactivation of CeO_2/TiO_2 catalysts for the SCR of NO with NH_3. When the molar ratio of Ca/Ce exceeded 1.1, the NO conversion fell below 40%. Fresh and CaO-doped catalysts were characterized by BET, XRD, XPS, H_2-TPR and NH_3-TPD. The results showed that the doping of CaO led to pore blockage, decrease in the concentration of Ce and NH_3 adsorption capacity on catalyst surface. The interaction among CaO, ceria and TiO_2 could cause transformation of Ce^{3+} to Ce^{4+}, decrease in surface adsorbed oxygen and degradation of redox ability and surface acidity. According to calculated DFT results, the creation and hydrogenation of oxygen vacancies were inhibited, thereby leading to the decrease in the proportion of Ce^{3+}. This was in good agreement with the XPS results. These factors contributed to the decline of the SCR activity over CeO_2/TiO_2 catalysts after doping CaO.

ACKNOWLEDGEMENTS

This work is financially supported by the National Natural Science Foundation of China (No. 51506226), Shandong Provincial Natural Science Foundation (No. ZR2015EM010) and the Fundamental Research Funds for the Central Universities (No. 15CX-05005A).

REFERENCES

1. J. P. Dunn, P. R. Koppula, H. G. Stenger and I. E. Wachs, *Appl. Catal. B*, **19**, 103 (1998).
2. M. Yates, J. A. Martín, M. Á. Martín-Luengo, S. Suárez and J. Blanco, *Catal. Today*, **107-108**, 120 (1996).
3. R. Guo, W. Zhen, W. Pan, Y. Zhou, J. Hong, H. Xu, Q. Jin, C. Ding and S. Guo, *J. Ind. Eng. Chem.*, **20**, 1577 (2014).
4. M. Luo, J. Chen, L. Chen, J. Lu, Z. Feng and C. Li, *Chem. Mater.*, **13**, 197 (2001).
5. X. Zhu, X. Gao, R. Qin, Y. Zeng, R. Qu, C. Zheng and X. Tu, *Appl. Catal. B*, **170-171**, 293 (2015).
6. R. Guo, Y. Zhou, W. Pan, J. Hong, W. Zheng, Q. Jin, C. Ding and S. Guo, *J. Ind. Eng. Chem.*, **19**, 2022 (2013).
7. W. Xu, Y. Yu, C. Zhang and H. Hong, *Catal. Commun.*, **9**, 1453 (2008).
8. X. Gao, Y. Jiang, Y. Zhong, Z. Luo and K. Cen, *J. Hazard. Mater.*, **174**, 734 (2010).
9. W. Shan, F. Liu, H. Hong, X. Shi and C. Zhang, *ChemCatChem.*, **3**, 1286 (2011).
10. J. P. Chen, M. A. Buzanowski and R. T. Yang, *J. Air Waste Manage. Assoc.*, **40**, 1403 (1990).
11. D. Nicosia, I. Czekaj and O. Kröcher, *Appl. Catal. B*, **77**, 228 (2008).
12. F. Tang, B. Xu, H. Shi, J. Qiu and Y. Fan, *Appl. Catal. B*, **94**, 71 (2010).
13. L. Chen, J. Li and M. Ge, *Catal. Eng. J.*, **179**, 531 (2011).
14. S. M. Mousavi, A. Niaei, M. J. I. Gómez, D. Salari, P. N. Panahi and V. Abaladejo-Fuentes, *Mater. Chem. Phy.*, **143**, 921 (2014).
15. H. Wang, X. Chen, S. Gao, Z. Wu, Y. Liu and X. Weng, *Catal. Sci. Technol.*, **3**, 715 (2013).
16. X. Gao, Y. Jiang, Y. Fu, Y. Zhong, Z. Luo and K. Cen, *Catal. Commun.*, **11**, 465 (2010).
17. B. Delley, *J. Chem. Phys.*, **113**, 7756 (2000).
18. A. Beltrán, J. R. Sambrano, M. Calatayud, F. R. Sensato and J. Andrés, *Surf. Sci.*, **490**, 116 (2001).
19. X. Q. Gong, A. Selloni and A. Vittadini, *J. Phys. Chem. B*, **110**, 2804 (2006).
20. T. Homann, T. Bredow and K. Jug, *Surf. Sci.*, **555**, 135 (2004).
21. A. D. Becke, *Phys. Rev. A*, **38**(6), 3098 (1988).
22. J. P. Perdew, K. Burke and0 M. Ernzerhof, *Phys. Rev. Lett.*, **77**(18), 3865 (1996).
23. B. Delley, *Phys. Rev. B*, **66**, 155125 (2002).
24. Y. Liu, T. Gu, Y. Wang, X. Weng and Z. Wu, *Catal. Commun.*, **18**, 106 (2010).
25. J. Fang, X. Bi, D. Si, Z. Jiang and W. Huang, *Appl. Surf. Sci.*, **253**, 8952 (2007).
26. Z. Wu, R. Jin, H. Wang and Y. Liu, *Catal. Commun.*, **10**, 935 (2009).
27. C. D. Wagner, W. M. Riggs, L. E. Davis, J. F. Moulder and G. E. Mullenberg, *Handbook of X-ray Photoelectron Spectroscopy*, Perkin-Elmer Corporation, Minnesota (1979).
28. W. Shan, F. Liu, H. He, X. Shi and C. Zhang, *Appl. Catal. B*, **115-116**, 100 (2012).

29. Y. Jiang, Z. Xing, X. Wang, S. Huang, X. Wang and Q. Liu, *Fuel*, **151**, 124 (2015).
30. Y. Jiang, Z. Xing, X. Wang, S. Huang, Q. Liu and J. Yang, *J. Ind. Eng. Chem.*, **29**, 43 (2015).
31. S. Yang, W. Zhu, Z. Jiang, Z. Chen and J. Wang, *Appl. Surf. Sci.*, **252**, 8499 (2006).
32. C. Liu, L. Chen, H. Chang, L. Ma, Y. Peng, H. Arandiyan and J. Hua, *Catal. Commun.*, **40**, 145 (2013).
33. Z. Wu, R. Jin, Y. Liu and H. Wang, *Catal. Commun.*, **9**, 2217 (2008).
34. L. Chen, J. Li and M. Ge, *J. Phys. Chem. C*, **113**, 21177 (2009).
35. J. Liu, Z. Zhao and J. Wang, *Appl. Catal. B*, **84**, 185 (2008).
36. P. Li, Y. Xin, Q. Li, Z. Wang, Z. Zhang and L. Zheng, *Environ. Sci. Technol.*, **46**, 9600 (2012).
37. Z. Ma, D. Weng, X. Wu and Z. Si, *J. Environ. Sci.*, **24**, 1305 (2012).
38. E. N. Ndifor, T. Garcia, B. Solsona and S. H. Taylor, *Appl. Catal. B*, **76**, 248 (2007).
39. D. Andreeva, R. Nedyalkova, L. Ilieva and M. V. Abrashev, *Appl. Catal. B*, **52**, 157 (2004).
40. Q. Liu, Z. Liu and C. Li, *Chin. J. Catal.*, **27**, 636 (2006).
41. X. Du, X. Gao, R. Qu, P. Ji, Z. Luo and K. Cen, *ChemCatChem.*, **4**, 2075 (2012).